Liquefaction risk analysis for artificially solidified ground

Kasama, Kiyonobu
Faculty of Engineering, Kyushu University

Zen, Kouki
Faculty of Engineering, Kyushu University

https://hdl.handle.net/2324/21819

Liquefaction risk analysis for artificially solidified ground

K. Kasama & K. Zen

Division of Civil and Structural Engineering, Faculty of Engineering, Kyushu University, Fukuoka, Japan

ABSTRACT: This paper presents a risk-based procedure for the liquefaction assessment of artificially solidified ground. In this paper, the liquefaction potential of artificially solidified ground is analyzed statistically using Monte Carlo Simulation of the nonlinear earthquake response analysis considering the spatial variability of soil properties. Damage cost induced by a partial liquefaction in the solidified ground is estimated based on the reduction of the seismic bearing capacity obtained by the random field numerical limit analyses. Finally, liquefaction risk curve is calculated by multiplying the liquefaction potential with the damage cost and the probability of earthquake. The main conclusions are as follows: 1) The spatial variability of soil properties in artificially solidified ground affects greatly the liquefaction fragility curve and liquefaction risk curve respectively. 2) Annual liquefaction risk increases with increasing the spatial variability of shear strength and also depends on the characteristic of earthquake hazard curve.

1 INTRODUCTON

Ground solidification technique such as pre-mixing (Zen et al., 1992) and permeable-grouting (e.g. Yamazaki et al., 2006) has been widely used in Japan for the purpose of liquefaction countermeasure against harbor facility. Pre-mixing technique has been used in reclamation works in Japan to mitigate liquefaction in reclaimed land. Permeable-grouting technique is newly developed method that grouts permeable chemical agent into ground under existing structure and then replaces pore water of ground with gel-like chemical materials in order to avoid pore water pressure increasing during earthquake.

Although there have been significant advances in the equipments and methods used for ground solidification techniques, there remains a high degree of spatial variability in in-situ mechanical properties of artificially solidified ground under the practical construction condition. Namely, the artificially solidified ground shows the spatial variability of mechanical properties such as shear modulus and liquefaction strength resulting from the inherent spatial variability of soil profile in original ground before solidification, the non-uniformities of mixing and grouting, etc. It is also reported by Zen et al. (1990) that sandy soils with small shear strength improved insufficiently by solidification technique show liquefaction failure as well as conventional sandy soil while solidified sandy soils with a large shear strength shows tensile failure as well as brittle material. Therefore, the effectiveness of ground solidification technique for mitigating liquefaction of sandy ground is considered to be affected by the spatial variability of soil properties such as the liquefaction strength in solidified ground.

This paper presents a risk-based procedure for the liquefaction assessment of artificially solidified ground. In this paper, the liquefaction potential of artificially solidified ground is analyzed statistically using Monte Carlo Simulation of the nonlinear earthquake response analysis considering the spatial variability of soil properties. Damage cost induced by a partial liquefaction in the solidified ground is estimated based on the reduction of the seismic bearing capacity obtained by the random field numerical limit analyses. Finally, liquefaction risk analysis was carried out by incorporating the liquefaction potential with the damage cost and an earthquake hazard curve.
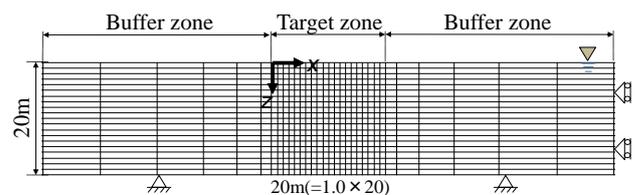

Fig.1 Finite element mesh

2 LIQUEACTION PROBABILITY ANALYSIS

2.1 *Analytical procedure*

Artificially solidified ground was modeled by two dimensional (2D) Finite Element Method as shown in Fig. 1, in which the spatial variability in liquefaction strength and shear wave velocity were expressed on the random theory. Dynamic shear stress in the ground was analyzed statistically through Monte Carlo simulation of the nonlinear earthquake response analysis (FLIP) developed by (Iai et al. 1990). The effects of inherent spatial variability in soil property are represented in the analyses by modeling the unconfined compressive
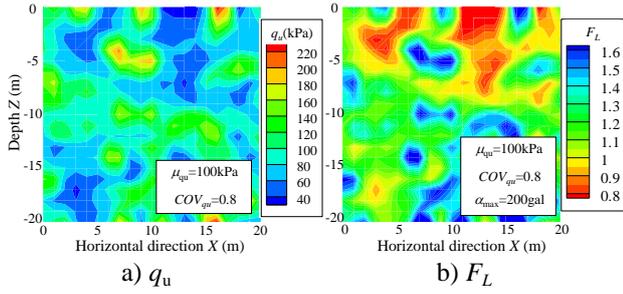
a) q_u b) F_L

Fig. 2 Typical results of strength and liquefaction

Table 1. Input parameters

Input parameter	Symbol	Unit	Value
Unconfined compressive strength	μ_{qu}	kPa	50-200
	COV_{qu}		0.2-1.0
Correlation length	θ	m	0.1
Poison ratio			0.33
Density	ρ	t/m^3	1.89
Damping coefficient	h		0.15
Internal friction angle	ϕ	degree	30
Unit weight	γ	kN/m^3	18.5
Effective unit weight	γ'	kN/m^3	8.5
Monte Carlo iteration			1000

strength q_u of solidified ground as a homogeneous random field (Vanmarcke, 1984). The unconfined compressive strength is assumed to have an underlying log-normal distribution with mean, μ_{qu}, and the coefficient of variation, $COVq_u$, and an isotropic scale of fluctuation (also referred to as the correlation length), θ. Fig. 2a) shows a typical distribution of q_u for target zone of finite element mesh for μ_{qu}=100kPa and $COVq_u$=0.4. It can be seen that spatial variability of strength was well modeled.

Table 1 summarized input parameters for nonlinear earthquake response analysis and Monte Carlo simulation. μ_{qu} was selected 50, 100 and 200 kPa which is corresponded to the strength required for conventional solidified ground to prevent liquefaction. $COVq_u$ for input parameter was selected to be 0.2, 0.4, 0.6 and 0.8 with the correlation length, θ, of 0.1m. In order to estimate shear wave velocity, V_s, as input parameter for the nonlinear earthquake response analysis from data set of q_u, Fig. 3 summarized the relationship between V_s and q_u for prior solidified soils. The correlation between V_s and q_u can be shown in Equation (1).

$$V_s = 10^{2.26} \cdot (q_u)^{0.21} \qquad (1)$$

After calculating V_s of each element based on the random theory, nonlinear seismic response analysis was performed to obtain maximum response acceleration, A_{max} for each element. The input wave for earthquake response analysis was the acceleration observed in the north-south direction at 65m depth in the 2005 Fukuoka-ken Seiho-oki Earthquake. The maximum input acceleration for bedrock, α_{max}, was adjusted at 100, 150, 200, 250, 300 and 450gal.
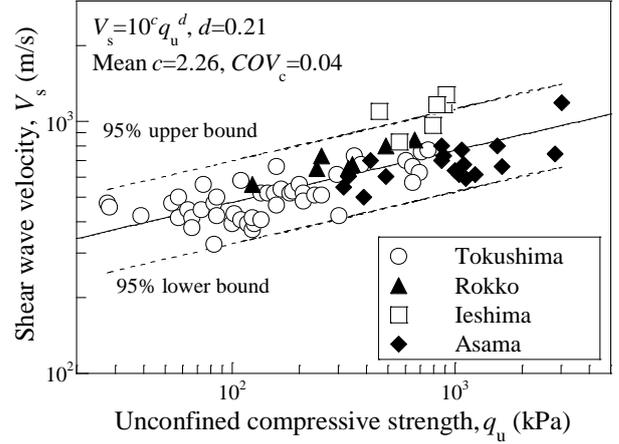

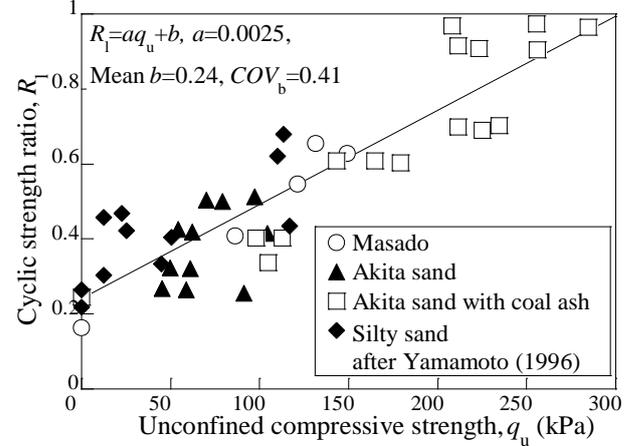Fig. 3 Shear wave velocity V_s and q_u

Fig. 4 Cyclic strength ratio R_l and q_u

In this paper, liquefaction safety factor, F_L, was used to judge the safety of liquefaction for each soil element. The liquefaction safety factor, F_L, is an index to evaluate the safety of soil element against liquefaction given by Equation (2).

$$F_L = R/L \qquad (2)$$

where R is a cyclic strength ratio of soil element against liquefaction and L is a cyclic stress ratio applied to the soil element. Generally, it is judged that soil element liquefies when F_L <1.0.

The liquefaction resistance, R, of soil element is estimated from q_u. It is general that R is equal to the stress ratio, R_l, which is the stress ratio at the number of loading cycles of 20 where liquefaction takes place in cyclic undrained triaxial test. Several simplified procedures for estimating R_l have been proposed, for example, using the results of standard penetration test (Tatsuoka et al., 1980., Liao et al., 1986) and cone penetration test (Toprak & Holzer, 2003). Fig. 4 shows the relationships between R_l and q_u from prior studies (Zen et al., 1990, Yamamoto et al., 1996) showing that R_l increases linearly with increasing q_u with some data scatters. Moreover, the relationships between R_l and q_u can be obtained by the following equation.

$$R = R_l = 0.0025 \cdot q_u + 0.24 \qquad (3)$$

Cyclic shear stress ratio, L, for each soil element was calculated from Equation (4).

$$L = A_{\max} / g \cdot \sigma_v / \sigma'_v \qquad (4)$$

where $A_{\max}$ is maximum response acceleration for soil element by seismic response analysis, g is a gravitational acceleration. A total over-burden pressure, σ_v, and a effective overburden pressure, σ'_v, are constant (non-stochastic) parameters as $\gamma = 18.5\text{kN/m}^3$ and $\gamma' = 8.5\text{kN/m}^3$, respectively.

Fig. 2b) shows the distribution of F_L in target-zone for Fig. 2a) indicating that local liquefaction occurred along weaker soil elements. In this paper, in order to evaluate local liquefaction quantitatively, a liquefaction potential, $L_P[F_L<1|\alpha]$, was defined as the volume ratio of soil elements showing liquefaction to the total ground for the input earthquake acceleration of α was calculated. Namely, $L_P[F_L<1|50\text{gal}] = 10\%$ means that 10% of the ground shows liquefaction when earthquake acceleration is 50gal.

2.2 Liquefaction potential

In order to evaluate the stochastic property of liquefaction potential through Monte Carlo simulation, the obtained $L_P[F_L<1|\alpha]_i$ can be reported for each realization, i, of the unconfined compressive strength field. Hence, the mean, μ_{Pr}, and standard deviation, σ_{Pr}, of $L_P[F_L<1|\alpha]$ were recorded through each set of Monte Carlo simulations, as follows:

$$\mu_{L_P} = \frac{1}{n}\sum_{i=1}^{n} L_P\left[F_L < 1.0 \mid \alpha\right]_i \qquad (5a)$$

$$\sigma_{L_P} = \sqrt{\frac{1}{n-1}\sum_{i=1}^{n}\left(L_P\left[F_L < 1.0 \mid \alpha\right]_i - \mu_{L_P}\right)^2} \qquad (5b)$$

In order to examine the distributed profile of liquefaction potential, Fig. 5 shows a 12-bin histogram of $L_P[F_L<1|\alpha]$ from one complete series of Monte Carlo simulations with $\mu_{qu} = 100\text{kPa}$, $COV_{qu} = 0.4$ and $\alpha_{max} = 200\text{gal}$. It can be seen that liquefaction occurred averagely at 27% of the ground. Kataoka et al (2009) reported that all of the $L_P[F_L<1|\alpha]$ simulations satisfy the χ^2 goodness-of-fit tests at a 5% significance level for normal and log-normal distributions.

In order to evaluate the influence of the spatial variability of q_u on the $L_P[F_L<1|\alpha]$, Fig. 5 shows average liquefaction potential μ_{LP} against maximum input acceleration α_{max}. It can be seen that μ_{LP} for a given α_{max} increases with increasing COV_{qu} suggesting that liquefaction area increases as the spatial variability of strength increases.
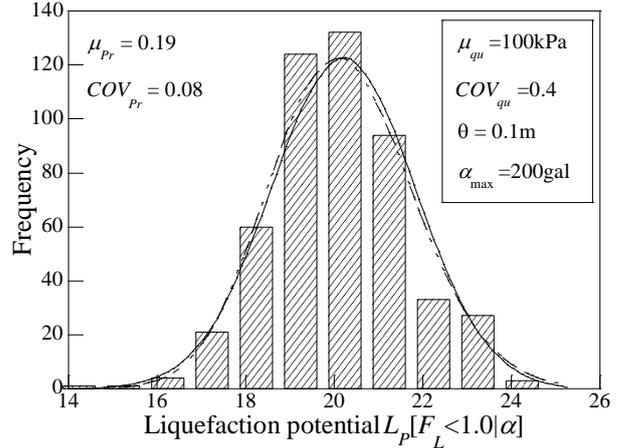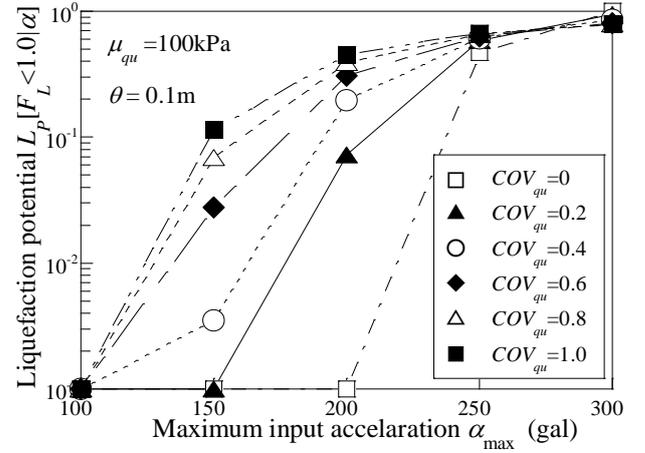

Fig. 5 Histogram of liquefaction potential

Fig. 6 Liquefaction potential and maximum input acceleration

3 LIQUEFACTION DAMAGE ANALYSIS

3.1 Random field numerical limit analyses

Damage cost C induced by liquefaction was estimated by multiplying a damage ratio K with the maximum damage cost C_0 which corresponded to atotal restoration cost when buildings and facilities on the ground are completely destroyed as follows:

$$C = C_0 \cdot K \qquad (6)$$

In this paper, damage ratio K is assumed to be determined by the reduction of bearing capacity due to liquefaction and seismic loading. Seismic bearing capacity was analyzed by the Numerical Limit Analyses considering the strength reduction induced by water pressure buildup induced by liquefaction, the spatial variability of shear strength and a seismic inertial force to ground and foundation induced by seismic horizontal acceleration.

The Numerical Limit Analyses (NLA) used in this paper were based on 2-D, plane strain linear programming formulations of the Upper Bound (UB) and Lower Bound (LB) theorems for rigid, perfectly plastic materials presented by Sloan and

Kleeman (1995) and Lyamin and Sloan (2002). One of the principal advantages of Numerical Limit Analyses is that the true collapse load is always bracketed by results from the upper and lower bound calculations. For example, Ukritchon et al. (1998) were able to achieve estimates of the collapse for footing under combinations of vertical, horizontal and moment loading to an accuracy ±5% for a wide range of undrained strength profiles in the underlying clay.

In order to consider the reduction of the shear strength, τ_f, due to water pressure buildup induced by liquefaction. The shear strength of soil element is given by:

$$\tau_f = (\sigma' - \Delta u)\tan\phi' = \sigma'(1 - \frac{\Delta u}{\sigma'})\tan\phi' \qquad (7)$$

where, Δu is a excess pore water pressure induced by the seismic acceleration. The excess pore water pressure ratio, $\Delta u/\sigma'$, in Equation (7) was assumed by the following Equation which is used in a design guideline for a common-use tunnel published by the Japan Road Association.

$$\frac{\Delta u}{\sigma'} = (F_L)^{-7} \qquad (8)$$

The seismic bearing capacity of the ground against a vertical loading is calculated by the numerical limit analysis after considering the reduction of the shear strength induced by the liquefaction using Equations (7) and (8). Moreover, the current calculation considers the increase in a horizontal inertial force to ground induced by seismic horizontal acceleration together with effects of strength reduction due to liquefaction mentioned above.

Figures 7a) and 7b) show the UB failure mechanisms against vertical loading. Each figure shows the deformed mesh, vectors of the UB velocity field, zone of plastic shear distortion (dark zones within in velocity field). It can be seen that the computed failure mechanisms is no longer symmetrical and shows a local failure passing through liquefaction regions of the solidified ground. It can be emphasized that the local failure mode of ground near the foundation is shown because of the local liquefaction induced by the spatial variability of soil properties in solidified ground.

3.2 Damage ratio and liquefaction potential

Damage ratio K was defined as the reduction of bearing capacity induced by water pressure buildup induced by liquefaction, the spatial variability of shear strength and a seismic inertial force to ground and foundation induced by seismic horizontal acceleration, as follows:

a) Deformed mesh

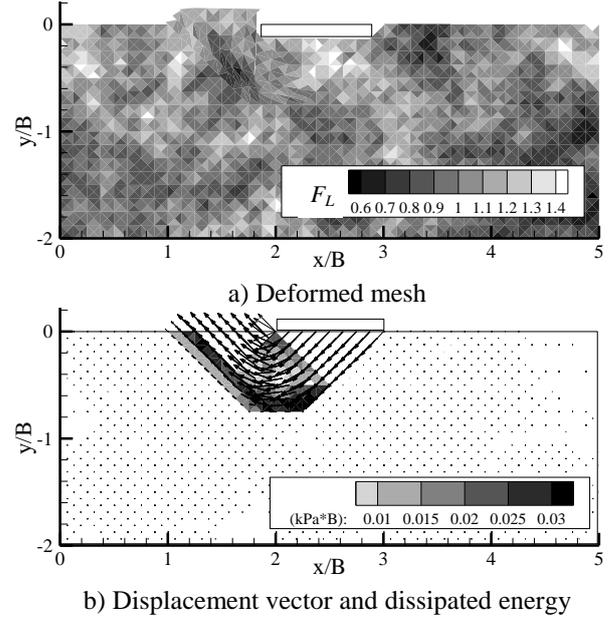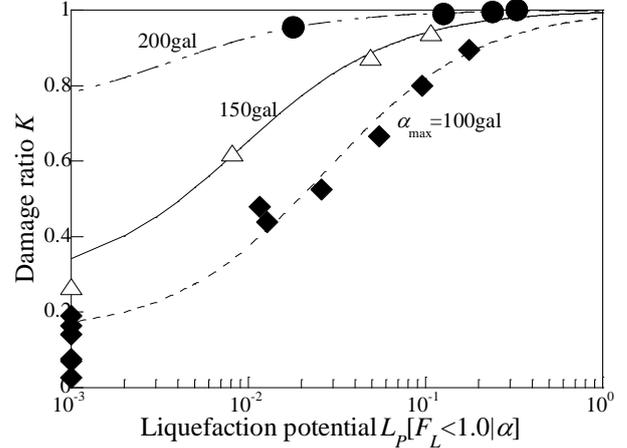b) Displacement vector and dissipated energy

Fig. 7 Deformed mesh, vectors of displacement and dissipated energy

Fig. 8 Damage ratio and liquefaction potential

Table. 3 Damage ratio and liquefaction potential

α_{max}	Damage ratio K	R
100gal	$K = x/(0.0313 + 0.0116 \times x) + 14$	0.9832
150gal	$K = x/(0.0124 + 0.0130 \times x) + 27$	0.9989
200gal	$K = x/(0.0127 + 0.0357 \times x) + 72$	0.9998

x: Liquefaction potential $L_P[F_L < 1.0|\alpha]$

$$K = 1.0 - \frac{N_\gamma}{N_{\gamma 0}} \qquad (9)$$

where $N_{\gamma 0}$ is a bearing capacity factor under normal condition while is $N_{\gamma 0}$ is a seismic bearing capacity factor.

In order to evaluate the effect of local liquefaction on the damage ratio K, Fig 8 shows the damage ratio K as a function of liquefaction potential and maximum horizontal acceleration. Damage ratio K increases with increasing liquefaction potential and maximum horizontal acceleration. Especially, Damage ratio K increases greatly when
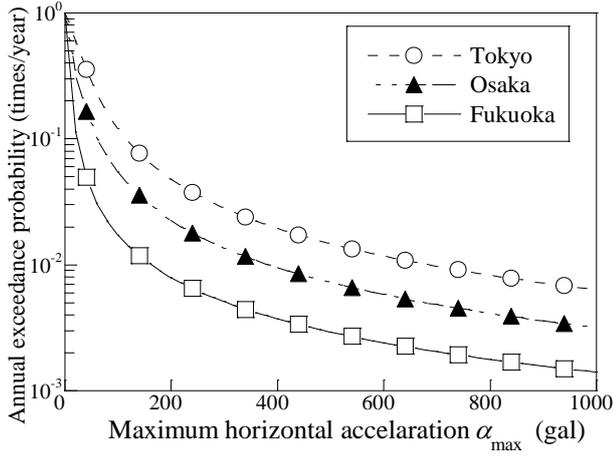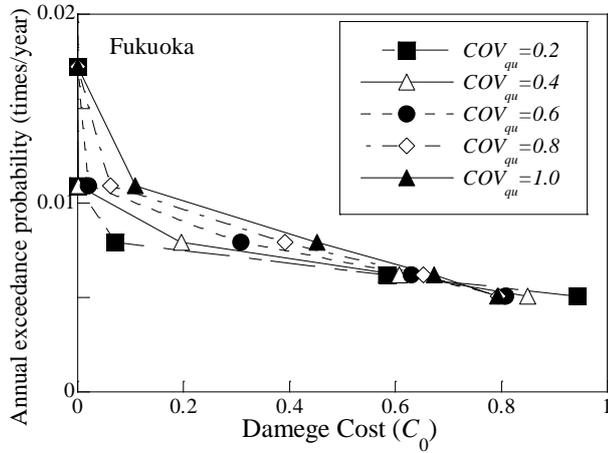
Fig. 9 Earthquake hazard curve

Fig. 10 Liquefaction risk curve

a) Fukuoka

b) Tokyo

Fig. 11 Annual liquefaction risk against $COVq_u$

liquefaction potential is up to 0.1 meaning that a local liquefaction is very sensitive to the seismic bearing capacity of solidified ground. Table 3 summarized the regression function of damage ratio and the correlation coefficient R. Kutsuna et al (2009) reported characteristics of seismic bearing capacity of solidified ground considering the spatial variability of liquefaction strength.
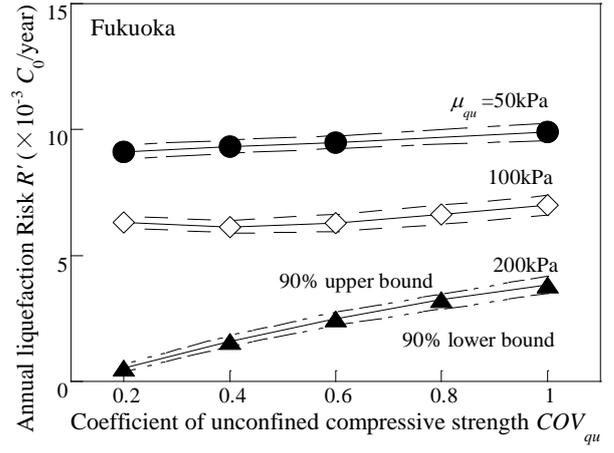
4 LIQUEFACTION RISK ANALYSIS

Liquefaction risk R was defined using the probability of liquefaction P and damage cost C induced by liquefaction, as follows:
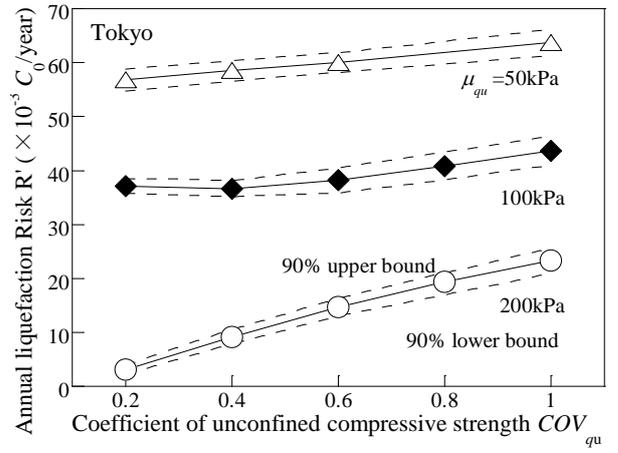
$$R = P \cdot C \qquad (10)$$

In the conventional risk analysis for earthquake, the occurrence probability of maximum horizontal acceleration α, $p(\alpha)$, was calculated based on the earthquake hazard curve which shows annual exceedance probability of maximum horizontal acceleration α, P_α, as follows:

$$p(\alpha) = -\frac{dP_\alpha}{d\alpha} \qquad (11)$$

Fig. 9 shows the earthquake hazard curve for Tokyo, Osaka and Fukuoka prefectures in Japan proposed by Ishikawa (1998). The annual exceedance probability for Tokyo is one order larger than that for Fukuoka. Expected maximum horizontal accelerations of Tokyo and Fukuoka for $P_\alpha = 10^{-2}$ times/year (the return period: 100 years) are 651gal and 160 gal respectively. One of the advantages of using the earthquake hazard curve is to take into account the uncertainty of the earthquake occurrence and the local characteristics of earthquake in the risk analysis. The probability of liquefaction P is calculated by the liquefaction potential $L_P[F_L<1|\alpha]$ and $p(\alpha)$, as follows:

$$P = L_P[F_L < 1.0 \mid \alpha] \cdot p(\alpha) \qquad (12)$$

Finally, Liquefaction risk R can be obtained by combining Equations (6), (10) and (12), as follows:

$$R = L_P[F_L < 1.0 \mid \alpha] \cdot p(\alpha) \cdot C_0 \cdot K(L_P[F_L < 1.0 \mid \alpha], \alpha) \qquad (13)$$

In the proposed method, liquefaction potential $L_P[F_L < 1.0 \mid \alpha]$ was a common index for both the

probability analysis and damage analysis in the risk analysis.

Fig. 10 shows the relationship between annual exceedance probability of liquefaction P for Fukuoka and damage const C which is known as a liquefaction risk curve in the field of risk analysis. The damage cost for a given annual exceedance probability increases as $COVq_u$ increases. In case of $P_\alpha = 10^{-2}$ times/year (the return period: 100 years), damage cost for $COV_{qu} = 1.0$ is $0.2*C_0$ while that for $COV_{qu} = 0.2$ is negligible. I can be characterized that the spatial variability of soil properties in artificially solidified ground affects greatly the liquefaction risk curve.

Fig. 11 shows annual liquefaction risk for Tokyo and Fukuoka. It is noted that annual liquefaction risk can be obtained as a size enclosed by liquefaction risk curve, vertical and horizontal axis in Fig. 10. In figure, 90% upper/lower bound limits are also shown. It can be seen that annual liquefaction risk increases with COV_{qu} increases while increase rate increases with increasing μ_{qu}. Annual liquefaction risks for Tokyo and Fukuoka are at most 7% and 1.2% of C_0 respectively which are relatively small risk. Therefore, it can be characterized that ground solidification technique is effective for reducing a liquefaction risk of irrespective of the spatial variability of soil properties in solidified ground.

5 CONCLUSIONS

This paper presents a risk-based procedure for the liquefaction assessment of artificially solidified ground. In this paper, the liquefaction potential of artificially solidified ground is analyzed statistically using Monte Carlo Simulation of the nonlinear earthquake response analysis considering the spatial variability of soil properties. Damage cost induced by a partial liquefaction in the solidified ground is estimated based on the reduction of the seismic bearing capacity obtained by the random field numerical limit analyses. Finally, liquefaction risk analysis was carried out by incorporating the liquefaction potential with the damage cost and an earthquake hazard curve.

The main conclusions are as follows:

1) The liquefaction potential and local liquefaction area of solidified ground increase with increasing the spatial variability of shear strength.

2) The liquefaction potential is an influential index to reduce the seismic bearing capacity of solidified ground. Current study suggests that the seismic bearing capacity decreases greatly when the liquefaction potential is up to 0.1.

3) The spatial variability of soil properties in artificially solidified ground affects greatly the liquefaction fragility curve and liquefaction risk curve respectively.

4) Annual liquefaction risk increases with increasing the spatial variability of shear strength and also depends on the characteristic of earthquake hazard curve. Annual liquefaction risks for Tokyo and Fukuoka are at most 7% and 1.2% of the total restoration cost respectively which are relatively small risk under current input parameters.

REFERENCES

Iai, S., Matsunaga, Y. and Kameoka, T. (1990). "Strain space plasticity model for cyclic mobility, *Report of Port and Harbour Research Institute*, 29(4), 27-56.

Ishikawa, Y. (1998). "Probabilistic scenario earthquakes and engineering applications for evaluation of low-frequency great earthquake." Doctoral thesis, Kyoto Univ., Japan.

Liao, S.S.C, Veneziano, D. and Whitman, R.V. (1988). "Regression models for evaluating liquefaction probability." *J. Geotech. Eng., ASCE*, 114(4), 389-411.

Kataoka, N., Zen, K., Chen, G., Kasama, K. and Hayashi, K. (2009). "Effects of spatial variability of cement-treated soil on liquefaction potential." *Proc., Int. Conf. on Performance-Based Design in Earthquake Geotechnical Engineering*, Tsukuba, Japan, 1249-1554.

Kutsuna, J., Zen, K., Chen, G. and Kasama, K. (2009). "Numerical limit analysis on the seismic bearing capacity of anti-liquefaction ground." *Proc., Int. Symp. on Ground Improvement Technologies and Case Histories*, Singapore, 411-418.

Tatsuoka, F., Iwataki, T., Tokida, K., Yasuda, S., Hirose, M., Imai, T. and Kon-no, M. (1980). "Standard penetration tests and soil liquefaction potential evaluation." *Soils & Foundations*, 20(4), 95-111.

Toprak, S. and Holzer, T.L. (2003). "Liquefaction potential index: field assessment." *J. Geotech. and Geoenvir. Eng.*, ASCE, 129(4), 315-322.

Sloan, S.W. (1988). "Lower bound limit analysis using finite elements and linear programming." *Int. J. Numer. Analyt. Meth. Geomech.*, 12(1), 61-77.

Sloan, S. W. and Kleeman, P. W. (1995). "Upper bound limit analysis using discontinuous velocity fields." *Comput. Methods Appl. Mech. Eng.*, 127, 293-314.

Ukritchon, B., Whittle, A. J. and Sloan, S.W. (1998). "Undrained limit analyses for combined loading of strip footing on clay." *J. Geotech. Eng.*, ASCE, 124(3), 265-276.

Vanmarcke, E. H. (1984). Random fields: analysis and synthesis. MIT press, Cambridge, Mass.

Yamamoto, T., Yamauchi, T. and Horibuchi, K. (1996). "Effect of grain size characteristics on the effectiveness of cement fixing agent method for preventing liquefaction of sand to silt deposits." *J. Geotech. Eng.*, JSCE, 541/III-35, 133-146 (in Japanese).

Yamazaki, H., Hayashi, K. and Zen, K. (2006). "New liquefaction countermeasure based on pore water replacement." *Proc. 16th Int. Conf. on Soil Mechanics and Geotechnical Engineering*, 4, 2741-2744.

Zen, K., Yamazaki, H. and Sato, Y. (1990). "Strength and deformation characteristics of cement treated sands used for premixing method." *Report of Port and Harbor Research Institute*, 29(2), 85-118 (in Japanese).

Zen, K., Yamazaki, H., Yoshizawa, H. and Mori, K. (1992). "Development of premixing method against liquefaction, *Proc. 9th Asian Regional Conf. on Soil Mechanics and Foundation Engineering*, 1, 461-464.